agriculture

MDPI

Article

Comparative Analysis of Particle Size Characteristics of Calcareous Soils Under Cultivated and Natural Conditions Based on Fractal Theory

Yilong Li [1], Zongheng Xu [1,2,*], Hongchen Ye [1], Jianjiao Bai [1], Xirui Dai [1] and Yun Zeng [1]

[1] Faculty of Geography, Yunnan Normal University, Kunming 650500, China; 2043206000345@ynnu.edu.cn (Y.L.)
[2] Key Laboratory of Plateau Geographic Processes and Environment Change of Yunnan Province, Kunming 650500, China
* Correspondence: 140079@ynnu.edu.cn

Abstract

This study examines the particle size distribution (PSD) of calcareous soils under cultivated and natural conditions in Chenggong District of Kunming, Yunnan Province, China, using single-fractal and multifractal analyses. Soil samples were collected from the profiles of both land use types, and the PSD parameters, organic matter, and total nitrogen were determined. Single-fractal analysis showed that the single-fractal dimension (D) was mainly influenced by the clay content, with higher clay fractions corresponding to larger D values. The generalized dimension spectrum revealed clear differences between natural and cultivated soils: natural soils exhibited greater sensitivity to probability density weight index(q) changes and a more compact particle distribution, whereas cultivation led to broader PSD ranges and higher heterogeneity. The ratio D_1/D_0 was negatively correlated with the clay content, and multifractal spectrum asymmetry (Δf) indicated that fine particles dominate the variability in deeper layers. Compared with natural soils, cultivated soils had higher organic matter and total nitrogen, reflecting the influence of fertilization and tillage on the soil aggregation and PSD. These findings demonstrate that fractal theory provides a sensitive tool for characterizing soil structural complexity and land use impacts, offering a theoretical basis for soil quality assessment and the sustainable management of calcareous soils.

Keywords: calcareous soil; soil particle size distribution; generalized dimension spectrum; multifractal spectrum

check for updates

Academic Editor: Ryusuke Hatano

Received: 16 July 2025
Revised: 28 August 2025
Accepted: 29 August 2025
Published: 31 August 2025

Citation: Li, Y.; Xu, Z.; Ye, H.; Bai, J.; Dai, X.; Zeng, Y. Comparative Analysis of Particle Size Characteristics of Calcareous Soils Under Cultivated and Natural Conditions Based on Fractal Theory. *Agriculture* **2025**, *15*, 1858. https://doi.org/10.3390/agriculture15171858

Copyright: © 2025 by the authors. Licensee MDPI, Basel, Switzerland. This article is an open access article distributed under the terms and conditions of the Creative Commons Attribution (CC BY) license (https://creativecommons.org/licenses/by/4.0/).

1. Introduction

The soil particle size distribution (PSD) exhibits high complexity and spatial variability. In particular, the PSD of cultivated soils serves as a sensitive indicator of the spatial heterogeneity in the soil properties under different land use regimes [1,2]. Understanding this variability remains a major challenge in agricultural land management and is essential for sustainable development and the efficient utilization of soil resources [3]. As a key physical property, the PSD reflects the combined effects of complex geological and biological processes. It indicates the degree of soil weathering and pedogenesis [4,5], and it is closely linked to the soil structure, hydrological processes, nutrient cycling, microbial activity, pollutant transport, and plant growth [6–9]. Moreover, the PSD directly affects soil

erosion and land degradation [10,11]. Therefore, quantitatively characterizing the PSD is a fundamental objective in soil physics research.

The PSD plays a critical role in soil water movement [12]. With the intensification of global climate change and the increasing frequency of extreme weather events, the significance of soil water retention and conductivity has grown [13]. Soil particles of varying sizes create pore spaces of different scales, thereby influencing the soil's water-holding capacity [14]. Clay-rich soils exhibit good water retention due to their high specific surface area and strong water adsorption capacity. In contrast, sandy soils, characterized by large pores, exhibit rapid drainage but low water retention [15]. Soil permeability, which governs water infiltration and groundwater recharge, is also influenced by the PSD: sandy soils are generally more permeable, while clay soils are less so [16,17]. The results indicate that the soil particle size and the relative proportions of clay, silt, and sand have a significant effect on soil permeability. Another key aspect of cultivated soil quality is nutrient cycling. The existing research has shown that long-term cultivation may impair nutrient cycling through the loss of organic matter and the degradation of the soil structure. The application of organic fertilizers can enhance microbial activity, thereby improving nutrient dynamics [18]. In contrast, forest soils tend to have higher organic matter content and more stable aggregate structures, which facilitate nutrient retention and cycling [19]. Hence, different land use types can significantly affect the soil particle composition and nutrient availability [20]. Soils consist of irregularly shaped particles that exhibit self-similarity and follow a power-law relationship between the particle size and mass—hallmarks of fractal geometry [21]. Multifractal theory provides an effective framework for describing the local irregularity and complexity of systems such as PSDs [22]. Compared with traditional single-fractal approaches, multifractal analysis goes beyond simple power-law scaling. It not only quantifies the heterogeneity of the PSD, thereby enhancing our understanding of the soil formation and evolution [23], but also serves as a bridge connecting the PSD to key soil functions, such as hydrological behavior and nutrient cycling [24]. This enables the characterization of the nested fractal properties of PSDs and the environmental factors that drive them [25–27]. Key descriptors derived from multifractal spectra include the Rényi spectrum (D(q)-q) and the singularity spectrum ($f(\alpha)$-α), from which several critical parameters can be extracted: the capacity dimension (D_0), information dimension (D_1), correlation dimension (D_2), singularity strength (α_0), and multifractal spectrum width (Δf) [28–31]. These parameters encode important information on the PSD, reflecting its heterogeneity as well as the degree of concentration, dispersion, and asymmetry. In the purple soil zone of the Three Gorges Reservoir area, a comparison of soils under different land use types revealed that forest soils exhibited the highest values of the D_0, D_1, and D_2, indicating the greatest heterogeneity. In contrast, the single-fractal dimension of forest soils was significantly lower than that of paddy fields, grasslands, orchards, and drylands, reflecting the larger mean particle size in forest soils. The single-fractal dimension has shown a positive correlation with the clay and silt contents [32]. In karst calcareous soils, artificial forest soils displayed higher D_0–D_2 and $\Delta\alpha$ values but lower D_0 values compared with natural forest soils. These changes suggest that afforestation in karst regions accelerates the loss of fine particles while increasing the local concentration of and variability in particles in low-probability regions, thereby driving the overall PSD toward a more homogeneous, coarse-particle structure [33]. Similarly, under different vegetation restoration types in karst calcareous soils, the generalized dimension spectrum (D(q)) decreased more sharply for $q < 0$ than for $q > 0$, indicating that particles in sparse regions of the PSD are more sensitive to environmental drivers. Moreover, the correlations of the D_0, D_1, D_1/D_0, and D_2 with soil particles were opposite to those of the single-fractal dimension. Among all vegetation types examined, walnut plantations exhibited

the largest $\Delta\alpha$ values, reflecting the highest degree of heterogeneity in the particle size distribution [34]. While multifractal methods have been widely applied to describe soil physical properties and pore structures, studies on the PSD of red calcareous soils from a multifractal perspective remain scarce.

The Chenggong District of Kunming, Yunnan Province, China, is underlain by carbonate bedrock, and, in combination with its distinctive hydrothermal conditions, it has developed extensive red calcareous soils [35]. These soils have supported the emergence of a world-renowned flower industry and fruit–vegetable production base, serving as an ecological buffer zone for Kunming [36]. In recent years, the rapid development of modern agriculture in the region has intensified the influence of cultivation on the soil quality, resulting in marked differences between cultivated and natural soils. The application of multifractal theory to the analysis of the soil particle size distribution (PSD) is a relatively novel and practical approach, but comparative studies between natural and cultivated soils within this framework remain lacking. Addressing this gap is particularly relevant to the needs of sustainable agricultural development in the current era [37]. Therefore, this study combines physicochemical soil analyses with multifractal theory to elucidate the impact of cultivation on the PSD of red calcareous soils in Wanxichong, Chenggong District, and to investigate differences in the multifractal spectra and associated parameters between natural and cultivated soils.

2. Materials and Methods

2.1. Overview of the Study Area

Wanxichong is located in central Yunnan Province, China, and is administratively part of Chenggong District, Kunming. The area lies on the eastern shore of Dianchi Lake and to the west of Liangwang Mountain. The topography is predominantly shaped by a bedrock lithology and a series of north–south-oriented faults, resulting in a belt-like distribution of mountainous terrain. Active tectonic uplift and subsidence have given rise to fluvial alluvial terraces and lacustrine platforms. The underlying bedrock is primarily composed of Permian carbonate rocks. Influenced by both the geological substrate and regional hydrothermal conditions, the landscape is mainly characterized by basalt erosion landforms, as well as sandstone and shale erosion features. The geographic coordinates of the study area range from 102°52′30″ to 102°52′36″ E longitude and from 24°48′34.5″ to 24°48′35″ N latitude (Figure 1). The region experiences a subtropical plateau monsoon climate, with native vegetation dominated by evergreen broad-leaved forests. The average annual precipitation is approximately 818 mm. The favorable hydrothermal conditions in Wanxichong have fostered diverse agricultural practices, particularly the cultivation of Pyrus pyrifolia (Baozhu pear), ornamental flowers, and vegetables. To investigate the effects of different land use types on the soil particle size characteristics while minimizing the influence of natural factors (climate, topography, biota, parent material, and time) on the soil formation, two sampling sites were selected within approximately 500 m of each other. These comprised a natural red calcareous soil sample (natural soil, hereafter referred to as NS) and a cultivated red calcareous soil sample (cultivated soil, hereafter referred to as CS), located at 24°48′35″ N, 102°52′30.00″ E and 24°48′34.5″ N, 102°52′36.48″ E, respectively. The NS site was situated on a natural slope, with the surface sparsely covered by herbaceous vegetation. The CS site was located on artificially cultivated terraced farmland, characterized by annual tillage and the application of chemical fertilizers. Both sites were situated on gentle slopes with an average inclination of approximately 15°.

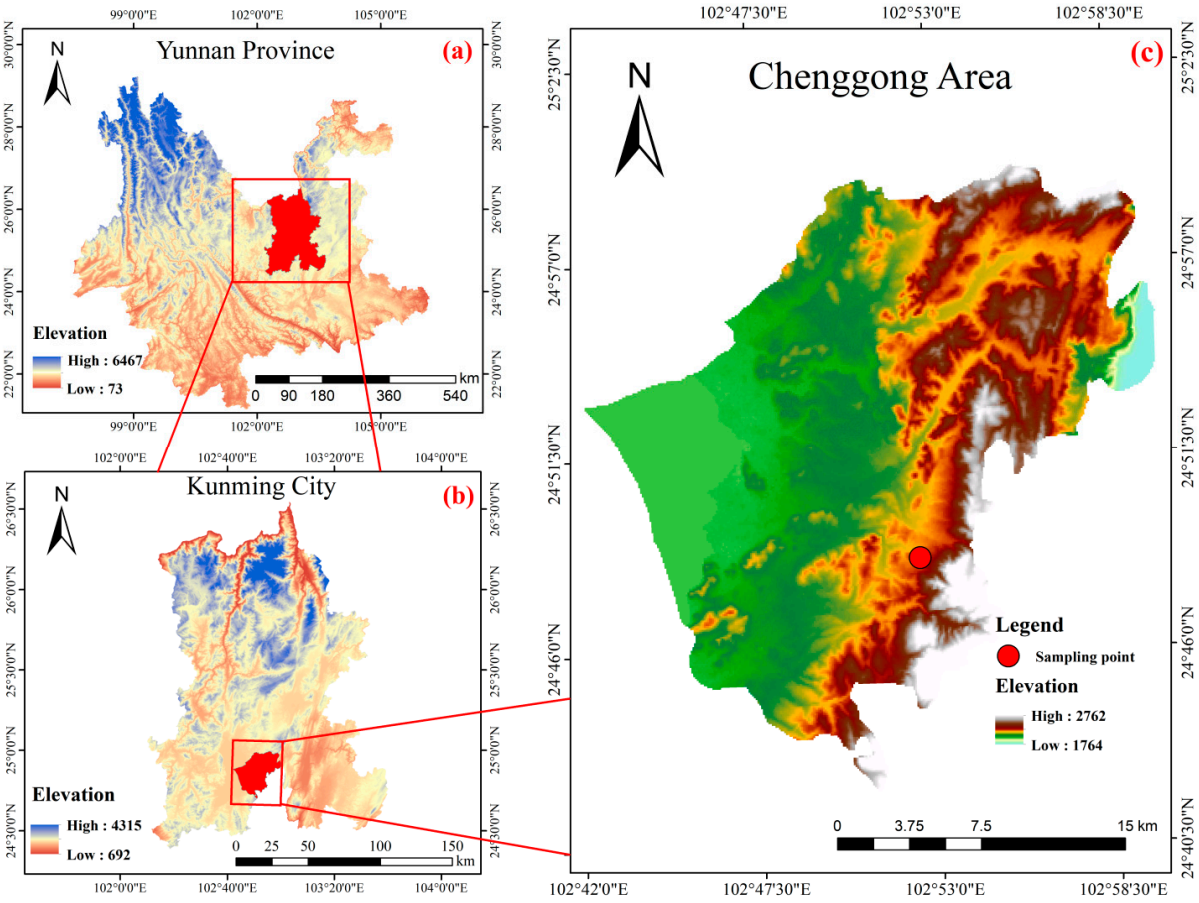

Figure 1. Sampling locations. (**a**) Yunnan Province; (**b**) Kunming city; (**c**) Chenggong area.

2.2. Soil Classification

The pedogenetic soil classification system has had a profound and long-standing influence in China and has been widely applied. Its fundamental concept emphasizes the interrelationship between soils, soil-forming factors, and the geographical landscape, using soil-forming factors and their impacts as the theoretical basis for classification. It also integrates pedogenic processes and soil properties as criteria for taxonomic differentiation. This system was once adopted in several Southeast Asian and Eastern European countries, and the soil classification system currently in use in China (1992) belongs to this pedogenetic framework. The Chinese soil classification system is highly intuitive, directly reflecting both the visible characteristics and the geneses of soils. According to this system, the soils in the present study are classified within the soil order Entisols (initial soils), the suborder Lithosols, and the subcategory of red calcareous soils within the Calcareous (limestone) soil group. This classification clearly indicates that the soils are developed from limestone parent material, consistent with the soil-geographical distribution pattern of the Yunnan–Guizhou Plateau. The red coloration reflects the desilication and enrichment in iron and aluminum under the subtropical plateau–montane monsoon climate.

2.3. Sampling and Sample Preparation

Soil profiles were excavated, and the vertical surfaces were cleaned to remove loose material. Fresh soil samples were collected vertically using a soil sampler at 20 cm intervals down to a depth of 100 cm. Five samples were taken from each profile and labeled wxc1-1 to wxc1-5 (for CS) and wxc2-1 to wxc2-5 (for NS). After labeling, the samples were sealed in core ring boxes, placed in opaque airtight bags, and stored under dark conditions to prevent moisture loss and light exposure.

In the laboratory, the samples were pretreated following standard procedures [38]. Air-dried soils were passed through a 2 mm sieve, and subsamples of 0.2–0.5 g were placed in small beakers. Each was treated with 10 mL of 10% hydrogen peroxide and heated to remove organic matter and disperse aggregates (Figure 2a). Deionized water was then added to the beakers, which were left undisturbed for 12 h. After decanting the supernatant, 10 mL of 0.05 mol/L sodium hexametaphosphate was added to achieve full particle dispersion. The soil particle size distribution was analyzed using a Mastersizer 2000 laser diffraction particle size analyzer (Malvern Instruments Ltd., UK), capable of measuring particles within the 0.02–2000 μm range (Figure 2b). Scanning electron microscopy (SEM) images were acquired using a ZEISS Sigma 300 field-emission scanning electron microscope (Carl Zeiss AG, Oberkochen, Germany), with a maximum magnification of 1,000,000×, allowing for the observation of particles as small as 1.0 nm. Organic matter and nitrogen can affect the soil particle size, so this study also conducted the determination of organic matter and nitrogen [39]. The soil organic matter content was determined using the potassium dichromate oxidation–external heating method. Air-dried soil (<0.25 mm, 0.10–0.50 g) was placed in a hard-glass tube, to which 5 mL of 0.8 mol L^{-1} $K_2Cr_2O_7$ solution and 5 mL concentrated H_2SO_4 were added. The mixture was gently swirled and then digested at 175 °C in a block digester. After cooling, the digest was transferred to an Erlenmeyer flask, and the tube was rinsed with 50 mL distilled water to bring the total volume in the flask to 60–80 mL. Following the addition of an o-phenanthroline indicator, the residual $K_2Cr_2O_7$ was titrated with standardized 0.20 mol L^{-1} $FeSO_4$ solution (Figure 2d), and the soil organic matter content was calculated based on the volume of titrant consumed [40], and the total nitrogen content was determined using the Kjeldahl digestion–distillation–titration method. Air-dried soil (<0.25 mm, 1.00 g) was placed in a Kjeldahl digestion tube, moistened with deionized water, and mixed with 6 g of catalyst (a ground mixture of 100 g K_2SO_4 and 10 g $CuSO_4 \cdot 5H_2O$) and 5 mL concentrated H_2SO_4. A reagent blank was included in each batch. Samples were digested on a graphite block digester until the digest became clear, cooled to room temperature, and analyzed using a Kjeldahl nitrogen analyzer (Hanon Instruments, Jinan, China) (Figure 2c). The distillate was titrated with standardized 0.010 mol L^{-1} HCl solution, and the total nitrogen content was calculated from the titration data [41]. The result data of the above samples were obtained during March 2022.

2.4. Calculation of Grain Size Characteristic Parameters

The commonly used parameters to describe grain size characteristics include the median grain size (Md), mean grain size (Mz), sorting coefficient (So), skewness (Sk), and kurtosis (Ku). Grain size frequency distributions were measured using a MasterSizer 2000 laser particle size analyzer, from which cumulative grain size curves were obtained. Representative points were selected from the curves, and their values were substituted into the equations listed in Table 1 to calculate the grain size characteristic parameters [42–45].

Table 1. The calculation methods of the particle size parameters.

Parameter	Calculation Formula
Median grain size (Md)	$M_d = \varphi_{50}$
Mean grain size (Mz)	$M_z = \frac{1}{3}(\varphi_{16} + \varphi_{84} + \varphi_{50})$
Sorting coefficient (So)	$S_o = \frac{\varphi_{84} - \varphi_{16}}{4} + \frac{\varphi_{95} - \varphi_5}{6.6}$
Skewness (Sk)	$S_k = \frac{1}{2}\left(\frac{\varphi_{84} + \varphi_{16} - 2\varphi_{50}}{\varphi_{84} - \varphi_{16}} + \frac{\varphi_{95} + \varphi_5 - 2\varphi_{50}}{\varphi_{95} - \varphi_5}\right)$
Kurtosis (Ku)	$K_u = \frac{\varphi_{95} - \varphi_5}{2.44(\varphi_{75} - \varphi_{25})}$

Note: φ_5, φ_{16}, φ_{25}, φ_{50}, φ_{75}, φ_{84}, and φ_{95} correspond to particle sizes at 5%, 16%, 25%, 50%, 75%, 84%, and 95% on the cumulative particle size distribution curve, respectively. Prior to analysis, particle sizes (in mm) were converted using the Krumbein phi scale: $\varphi = -\log_2(d)$, where φ is the Krumbein phi value and d is the particle diameter in millimeters.

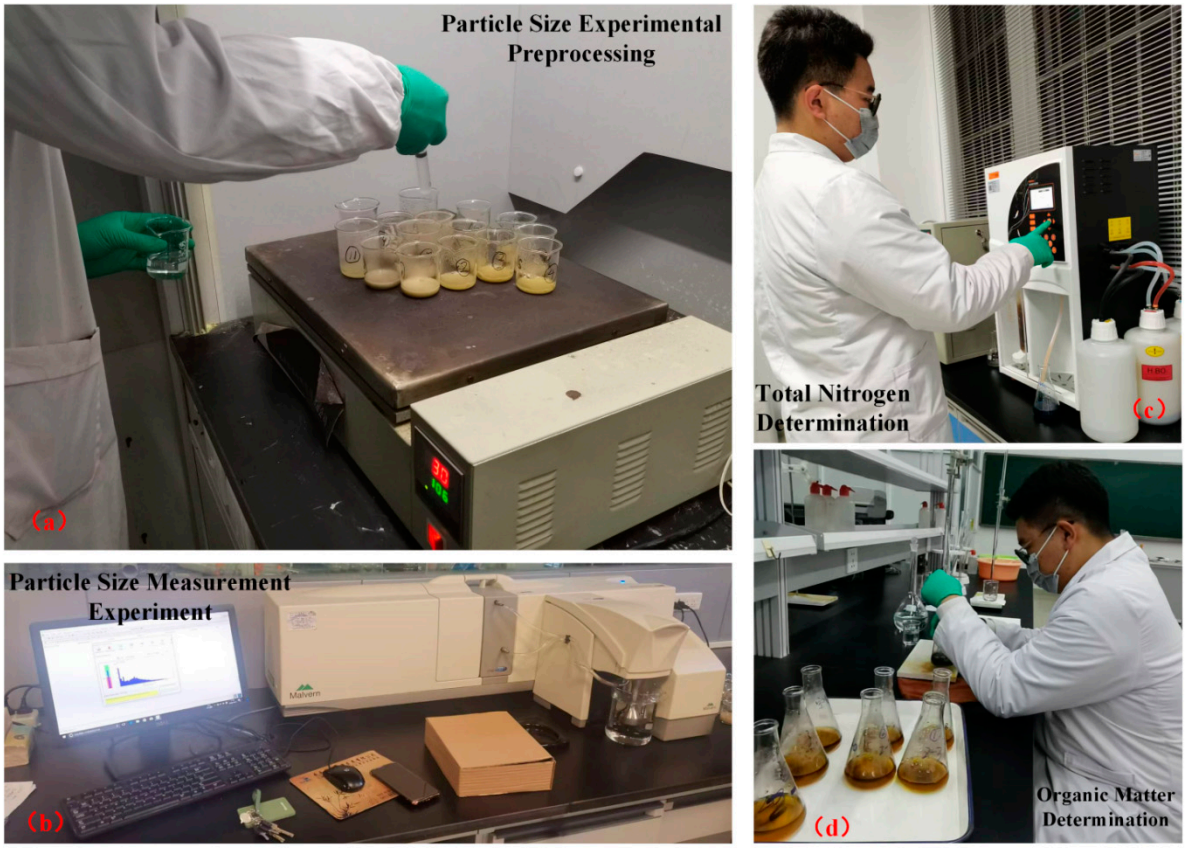

Figure 2. Measurement of particle size and chemical properties of lime soil. (**a**) Particle size experimental preprocessing; (**b**) particle size measurement experiment; (**c**) total nitrogen determination; (**d**) organic matter determination.

2.5. Analytical Method for Determining Single-Fractal Dimension of Soil Particle Size Distribution

The single-fractal dimension theory of PSD provides a simple and effective method for quantitatively characterizing the soil structure by fitting PSD data to a power-law model, in which the exponent corresponds to the single-fractal dimension. In this study, the power-law exponent method [46] is also employed. Assuming a constant soil density and a particle mass proportional to the cube of its radius, the single-fractal dimension is calculated based on the measured particle diameter (d) and its volume fraction ($V_{(d<r)}$) to compute $\lg\frac{V(d<r)}{V_0}$. Then, $\lg\frac{d_r}{d_{max}}$ is used as the *x*-axis and $\lg\frac{V_{(d<r)}}{V_0}$ is used as the *y*-axis. A linear regression is performed using the least-squares method, and the calculation model is as follows:

$$(3 - D)\lg\frac{d_r}{d_{max}} = \lg\frac{V_{(d<r)}}{V_0} \quad (1)$$

In the equation, d represents the calculated particle size of the soil (μm), d_r is the particle diameter (μm), d_{max} denotes the maximum particle diameter of the soil (μm), $V_{(d<r)}$ is the cumulative volume of soil particles with a diameter smaller than d_r (μm^3), V_0 is the total soil volume (μm^3), and D is the volumetric single-fractal dimension of the soil particle size distribution. After performing the linear regression based on the above equation, the slope (k) is obtained, and the fractal dimension is calculated as D = 3 − k.

2.6. Multifractal Analysis Method of Soil Particle Size Distribution

Soil is composed of solid particles of various shapes and sizes and is considered a porous medium system characterized by an irregular morphology and a self-similar structure [47]. The multifractal theory effectively reveals the heterogeneous properties of

such systems by capturing the uniformity and structural characteristics of PSDs. Compared with single-fractal models, multifractal analysis describes local features and their evolution across multiple scales using spectrum functions. Combined with statistical physics methods, it discloses the probability measure distributions of characteristic parameters and analyzes global structural features from a local perspective, making it especially suitable for studying the structures of complex soil systems [48,49].

In this study, continuous partitioning of an interval (I) was performed using binary scaling and a given total length (L). A K-th order binary division (K = 1, 2, 3, . . .) generated $N(\varepsilon) = 2^k$ equally sized subintervals, each with a size of $\varepsilon = L \times 2^{-k}$, to cover the entire interval (I). Based on the actual conditions of this research, K was set from 1 to 5. The PSD interval (I = [0.02, 2000] μm) was divided into 32 subintervals (I_i (i = 1, 2, . . ., 32)), with the length of each interval calculated as $I_i = \lg(\varphi_{max}/\varphi_{min})/32$, where φ_{min} and φ_{max} denote the minimum and maximum volume percentages of soil particles in this dataset, respectively. To ensure a uniform interval length, a new dimensionless distribution interval was constructed as $L = \lg(\varphi_{max}/\varphi_{min})$. This interval was then divided into $N(\varepsilon) = 2^k$ subintervals (I_i), each with the size $\varepsilon = L \times 2^{-k}$, where each subinterval contains at least one measurement. The measure $\mu_i(\varepsilon)$ represents the sum of all measurements within the subinterval (I_i). The probability density weight index (q) ranges from −10 to 10, with an increment of 0.5. Using the formula based on Rényi entropy [50], the generalized dimension (D(q)) can be calculated as follows:

$$D(q) \approx \frac{1}{q-1} \times \frac{\log\left[\sum_{i=1}^{N(\varepsilon)} \mu_i(\varepsilon)^q\right]}{\log \varepsilon} (q \neq 1) \quad (2)$$

$$D_1 \approx \frac{\sum_{i=1}^{N(\varepsilon)} \mu_i(\varepsilon) \log \mu_i(\varepsilon)^q}{\log \varepsilon} \ (q = 1) \quad (3)$$

In the equation, D(q) denotes the generalized dimension spectrum calculated according to the corresponding formula, which reflects the local characteristics and heterogeneity of the soil. Based on the computed values at different ε scales, the slope of the numerator and denominator is determined and then divided by the parameter $q - 1$, resulting in the D(q) value under the given parameter (q). The Rényi entropy (D(q)) exhibits a monotonically decreasing spectrum when the parameter (q) lies within the interval [–∞,+∞]. When $q \geq 1$, highly aggregated information is amplified. When $q \leq -1$, sparsely aggregated information is amplified [48,49].

The singularity exponent and the corresponding multifractal spectrum function can also be derived using the real-valued parameter (q) [51]:

$$\alpha(q) = \lim_{\varepsilon \to 0} \frac{\sum_{i=1}^{N(\varepsilon)} \mu_i(q,\varepsilon) \lg \mu_i(\varepsilon)}{\lg \varepsilon} \quad (4)$$

$$f(\alpha(q)) = \lim_{\varepsilon \to 0} \frac{\sum_{i=1}^{N(\varepsilon)} \mu_i(q,\varepsilon) \lg \mu_i(q,\varepsilon)}{\lg \varepsilon} \quad (5)$$

The singularity exponent ($\alpha(q)$) characterizes the local fractal properties of the soil spatial distribution. In combination with the multifractal spectrum function ($f(\alpha(q))$), it offers a comprehensive depiction of the detailed local heterogeneity in soil patterns. The width of the singularity spectrum ($\Delta\alpha(\Delta\alpha = \alpha_{max} - \alpha_{min})$) provides a quantitative measure of the spatial heterogeneity in the distribution of soil particle structures [52]. The multifractal spectrum function ($f(\alpha(q))$) serves to represent the complexity and non-uniformity of the soil spatial distribution [53], capturing the distribution patterns of different soil particle size classes (multifractal spectrum asymmetry: $\Delta f = f(\alpha_{min}) - f(\alpha_{max})$). When

$\Delta f < 0$, the particles with a lower volumetric fraction within the soil particle size distribution play a dominant role in the spatial variability in the soil distribution, resulting in a right-hook-shaped spectrum. When $\Delta f > 0$, the particles with a higher volumetric fraction within the soil particle size distribution play a dominant role in the spatial variability in the soil distribution, resulting in a left-hook-shaped spectrum [54]. α_0 is the mean singularity strength of the multifractal structure, which is related to the local density of the PSD. A lower α_0 value indicates a higher degree of local aggregation in the soil distribution [55].

2.7. Statistics

Statistical analyses were conducted using OriginPro 2023 (OriginLab Corp., Northampton, MA, USA). Linear regression models were employed to evaluate the effects of the soil particle size fractions (clay, silt, and sand contents) on the single-fractal dimension, with the coefficient of determination (R^2) used to assess the goodness of fit. All correlation analyses were performed in R software (version 4.5.0; R Core Team, Vienna, Austria). Pearson correlation coefficients were calculated to examine the relationships among the soil particle size fractions, multifractal parameters, and particle size descriptive indices (e.g., the Mz, TN, and OM). The correlation structure was visualized using the corrplot package, which provides a matrix-based graphical representation of correlation coefficients. To further explore similarity patterns among the variables, hierarchical clustering was performed based on Ward's D2 method, which minimizes within-cluster variance.

3. Results and Analysis

3.1. Characteristics of Particle Size Distribution

The particle size frequency distribution curves, presented in Figure 3a,c, show that both CS and NS exhibit similar unimodal patterns with relatively low contents at both ends of the distribution. The PSD range for CS spans from 2.86 φ to 13.22 φ. The modal particle sizes of the five CS samples are 12.42 φ, 11.62 φ, 12.42 φ, 12.42 φ, and 12.62 φ, with corresponding contents of 12.84%, 4.83%, 12.36%, 10.22%, and 18.69%, respectively. For NS, the PSD range is from 3.25 φ to 13.61 φ, with modal particle sizes of 12.42 φ, 12.42 φ, 12.42 φ, 12.62 φ, and 12.42 φ and respective contents of 10.22%, 8.22%, 12.67%, 16.42%, and 10.11%.

The cumulative particle size distribution curves, shown in Figure 3b,d, indicate that NS samples exhibit a smooth and consistent transition in their cumulative content from surface to deeper layers, following the general trend of the decreasing particle size with depth, with the curves remaining closely aligned between layers. In contrast, CS samples, influenced by mechanical fragmentation (frequent tillage) and chemical weathering (e.g., fertilizer and pesticide application), contain finer particles at the surface than NS. For example, when comparing wxc1-1 (CS) and wxc2-1 (NS) at a particle size of 12.03 φ, the CS content is 58.92%, markedly higher than the NS content of 45.57%, reflecting a stronger anthropogenic influence. Furthermore, fine particles in CS extend to greater depths than those in NS; comparison of the cumulative PSD curves shows that wxc1-5 (CS) is distinctly more concentrated in fine particles than wxc2-5 (NS).

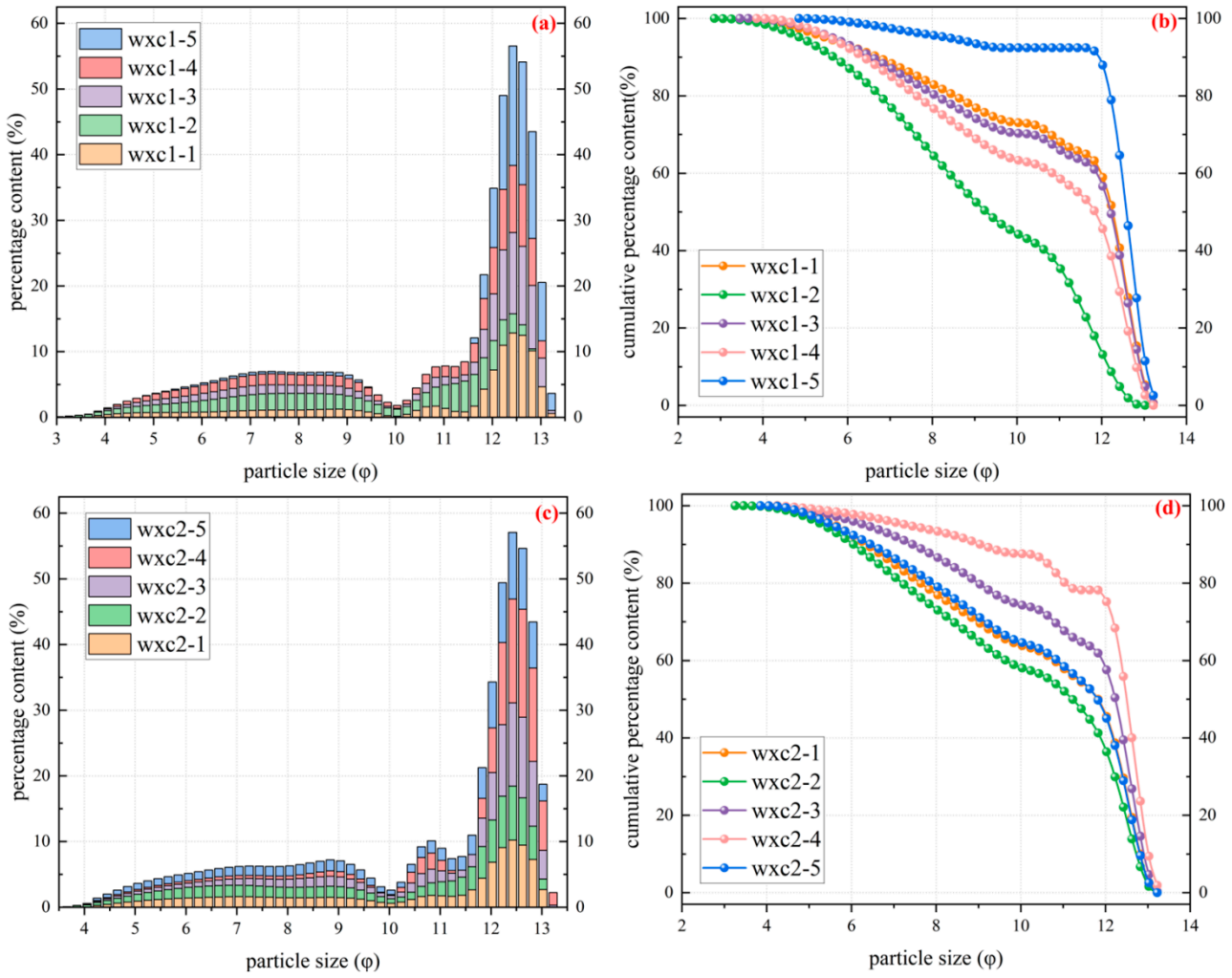

Figure 3. Particle size frequency and cumulative distribution curves. (**a**) CS frequency distribution curve; (**b**) CS cumulative frequency curve; (**c**) NS frequency distribution curve; (**d**) NS cumulative frequency curve.

3.2. Analysis of Particle Size Characteristics Based on Multiple Granulometric Indices

3.2.1. Texture Characteristics

Based on the particle size frequency distribution and following the USDA soil texture classification system, the red lime soils were categorized into three particle size classes: clay (<2 μm), silt (2–50 μm), and sand (>50 μm). According to the USDA soil texture triangle, the soils from the two land use types examined in this study are classified as sandy loam and silt loam, respectively (Figure 4). Among the analyzed samples, eight were identified as loam soils, and two deep-layer samples were classified as loam. Since soil texture classification is based solely on the percentage composition of the three primary particle size fractions, it may overlook certain local features of the particle size distribution. Consequently, the differentiation in the soil texture between the two land use types is not prominent. Therefore, additional quantitative indices are required to further interpret and compare the differences in the particle size characteristics between the two soil types.

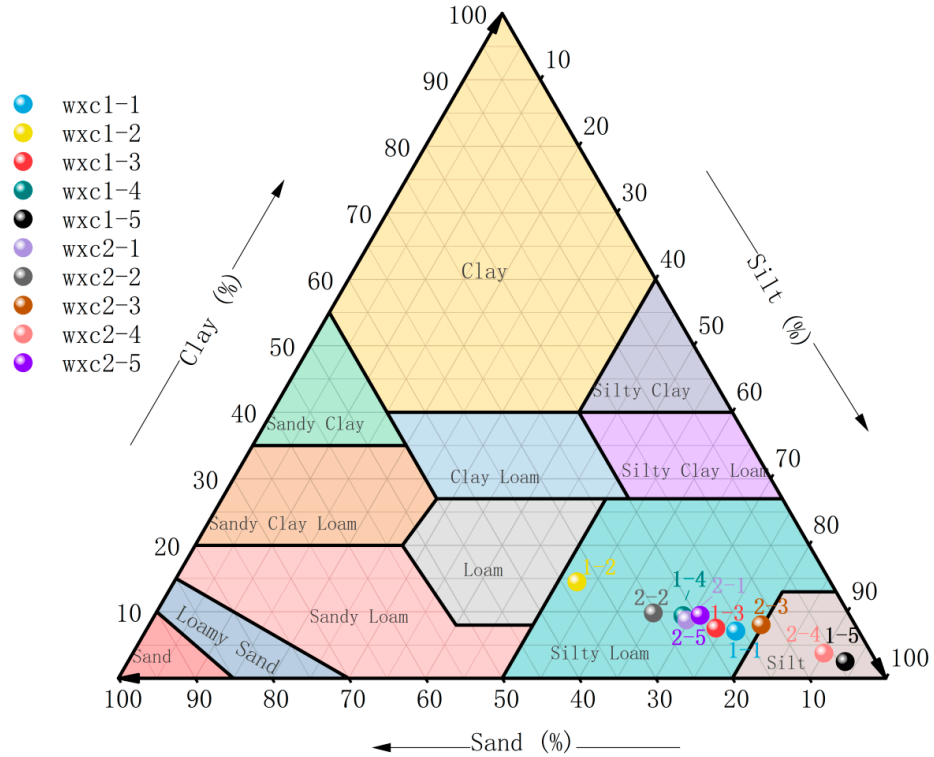

Figure 4. Soil texture classification in Wanxichong.

3.2.2. Characteristics of Grain Size Parameters

Commonly, the particle size distribution is characterized using the median grain size [56] (Md), mean grain size (Mz), sorting coefficient [57] (So), skewness (Sk), and kurtosis (Ku). As shown in Figure 5a,c, the Md in CS ranged from 9.08 φ to 12.38 φ and the Mz ranged from 8.99 φ to 12.36 φ, whereas in NS, the Md ranged from 11.02 φ to 12.30 φ and the Mz ranged from 9.98 φ to 11.85 φ. Both soil groups showed decreasing grain sizes with increasing depth, along with narrowing distribution intervals. The So in CS was generally close to 2.5, except for the deepest sample, wxc1-5, which had a value of 0.93. In NS, the So ranged from 1.42 to 2.60 (Figure 5a,c). For the Sk, the CS values ranged from −0.79 to −0.11, while the NS values ranged from −0.75 to −0.55 (Figure 5b,d). Ku analysis indicated that CS sample wxc1-5 and NS sample wxc2-4 exceeded a value of 3, whereas the other samples ranged between 0 and 1 (Figure 5b,d). Regarding soil nutrients, the OM in CS ranged from 12.58 to 19.76 $g \cdot kg^{-1}$ and the TN ranged from 0.056 to 0.0728 $g \cdot kg^{-1}$, while in NS, the OM ranged from 1.2 to 12.58 $g \cdot kg^{-1}$ and the TN ranged from 0.0168 to 0.0658 $g \cdot kg^{-1}$.

Compared with NS, CS exhibited a wider particle size distribution, reflecting greater variability induced by cultivation. Most CS layers showed poorer sorting, whereas NS displayed relatively better sorting, likely due to natural vegetation promoting aggregate formation and limiting the exposure of coarse particles. The Sk values suggest that surface tillage in CS exposed coarse particles, though the distribution remained dominated by fine fractions; in NS, the strong negative Sk indicates clay dominance and a negligible sand content. Ku further revealed that specific layers contained very high clay proportions with leptokurtic distributions, while the majority of samples exhibited weakly peaked distributions dominated by clay with 20–30% silt. For soil fertility, CS showed substantially higher OM and TN contents than those of NS. These differences are attributable to agricultural inputs such as crop residue incorporation, organic fertilization, and nitrogen amendments. In contrast, the OM and TN in NS primarily originated from litterfall, with subtropical climatic conditions accelerating decomposition and promoting nitrogen losses through

leaching and denitrification. Although both soil types experienced nutrient loss, cultivation significantly enhanced the TN concentrations in CS.

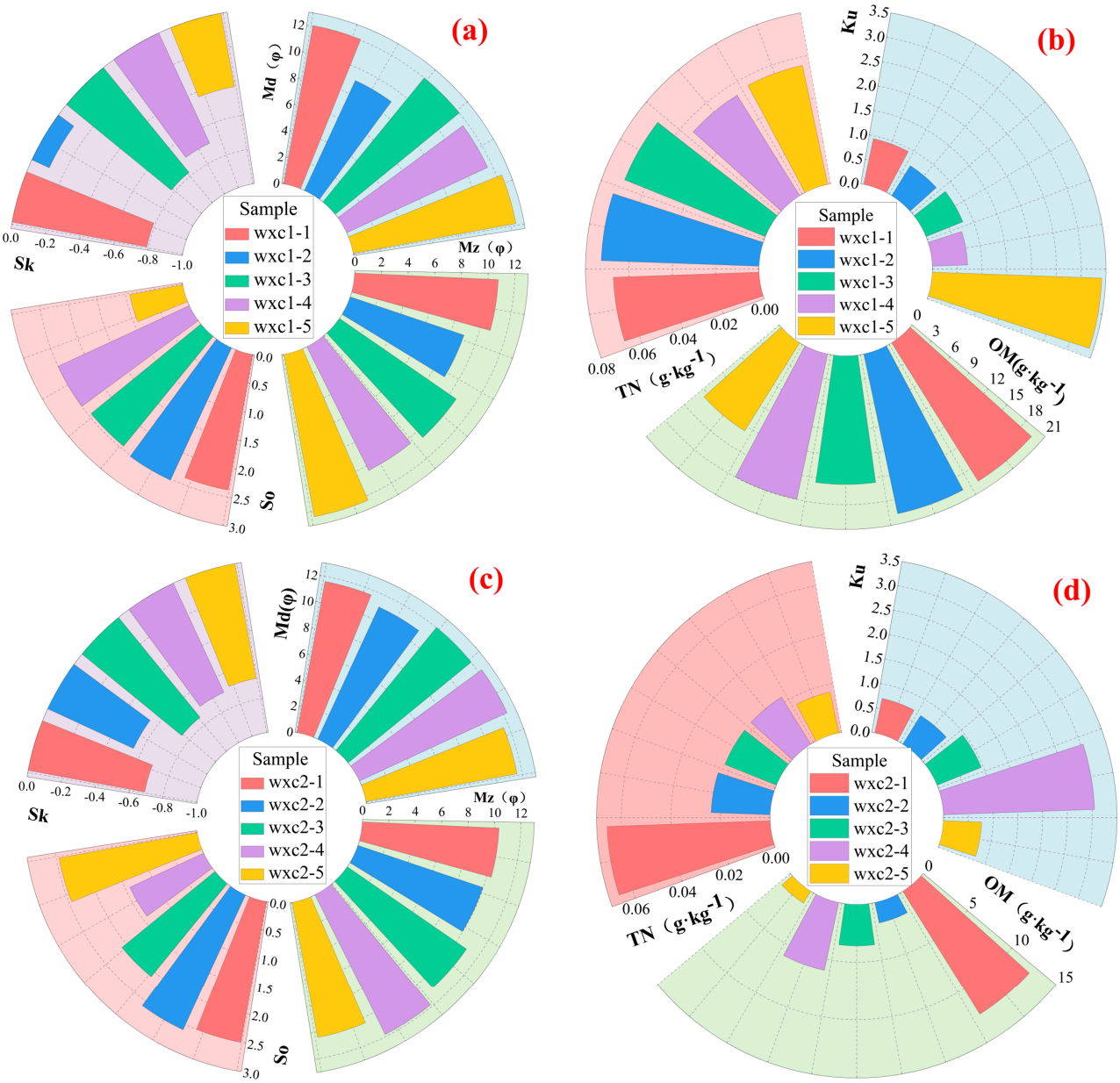

Figure 5. Characteristic rose diagram of grain size indicators. (**a**,**b**) Characteristics of CS parameters; (**c**,**d**) characteristics of NS parameters.

3.2.3. Characteristics of Single-Fractal Dimension

The single-fractal dimension quantitatively characterizes the structural composition of the soil particle size fractions. Together with the grain size parameters, it provides a sensitive indicator of the soil structure. A higher value reflects greater self-similarity in particle distributions. The power-law method was applied to calculate the single-fractal dimension. Based on the principles of volume percentage measurement by laser particle size analyzers, the cumulative volume percentage of particles with diameters smaller than r was plotted against r on a double-logarithmic scale. The slope (k) of the fitted line (least-squares regression) was then used to compute the single-fractal dimension as $D = 3 - k$.

The calculated results (Table 2) show that the single-fractal dimension (D) of both CS and NS samples falls between 2 and 3, consistent with the theoretical range for three-dimensional structures [58]. All samples thus exhibit fractal self-similarity.

Table 2. The number of global and local shape dimensions of each domain.

	wxc 1-1	wxc 1-2	wxc 1-3	wxc 1-4	wxc 1-5	wxc 2-1	wxc 2-2	wxc 2-3	wxc 2-4	wxc 2-5
D	2.75	2.60	2.74	2.76	2.81	2.75	2.73	2.71	2.80	2.75
D_{Clay}	2.14	1.70	2.12	2.33	2.38	2.33	2.20	2.06	2.31	2.30
D_{Cup}	2.93	2.86	2.92	2.89	2.98	2.89	2.89	2.94	2.97	2.91

To further investigate domain-specific features, fractal dimensions were computed separately for the entire particle size domain (D), the clay fraction (<2 μm, D_{Clay}), and the combined silt—sand fraction (>2 μm, D_{Cup}). As shown in Figure 6, regression fits were better in the silt—sand fraction than those in the clay fraction for both CS and NS. In CS, the silt—sand data (Figure 6c) aligned more closely with the fitted line than clay data (Figure 6a). A similar trend was observed in NS (Figure 6b,d). The determination coefficients (R^2) in Table 3 confirm this: R^2 values in the clay fraction ranged from 0.41 to 0.65, while those in the silt—sand fraction exceeded 0.9. Referring back to Table 2. The overall fractal dimension (D) generally ranged between 2.7 and 2.8, while the DClay ranged from 2.0 to 2.3. Excluding clay increased the DCup to ~2.9, approaching the D. This reflects the narrow size distribution and high cumulative percentage of clay, which reduced the regression slopes, compared to the broader distribution of silt and sand, which produced steeper slopes.

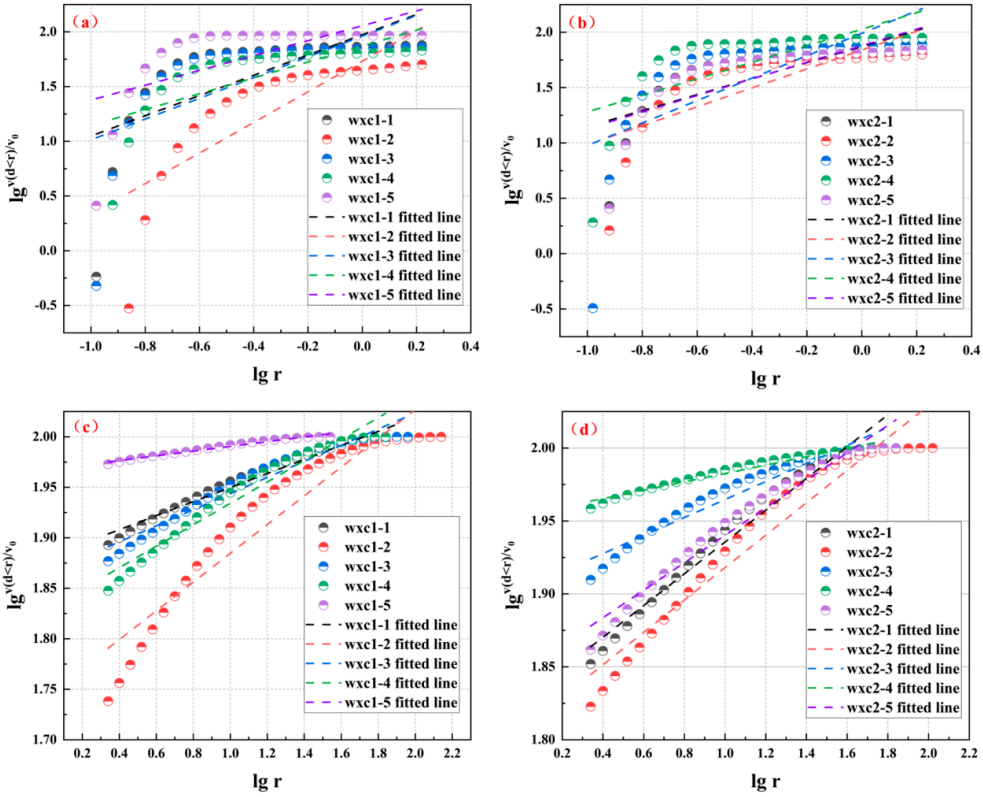

Figure 6. Fractal dimension calculations for soil particles across different grain size ranges. (**a**) Fractal dimension of the clay fraction in cultivated soil; (**b**) fractal dimension of the clay fraction in natural soil; (**c**) fractal dimension of the silt and sand fractions in cultivated soil; (**d**) fractal dimension of the silt and sand fractions in natural soil.

Table 3. Linear fitting regression equation and decision coefficient (R^2) of fractal dimension of clay and silt.

Scheme 2	Linear Regression Equation for the Fractal Dimension of the Clay Fraction	R^2	Linear Regression Equation for the Fractal Dimension of the Silt– and Sand Fractions	R^2
wxc1-1	$lg^{v(d<r)/v0}$ = 0.86lgr + 1.93	0.44	$lg^{v(d<r)/v0}$ = 0.07lgr + 1.88	0.97
wxc1-2	$lg^{v(d<r)/v0}$ = 1.30lgr + 1.68	0.65	$lg^{v(d<r)/v0}$ = 0.14lgr + 1.74	0.90
wxc1-3	$lg^{v(d<r)/v0}$ = 0.88lgr + 1.92	0.44	$lg^{v(d<r)/v0}$ = 0.08lgr + 1.86	0.95
wxc1-4	$lg^{v(d<r)/v0}$ = 0.67lgr + 1.84	0.53	$lg^{v(d<r)/v0}$ = 0.11lgr + 1.83	0.96
wxc1-5	$lg^{v(d<r)/v0}$ = 0.62lgr + 2.02	0.41	$lg^{v(d<r)/v0}$ = 0.02lgr + 1.97	0.98
wxc2-1	$lg^{v(d<r)/v0}$ = 0.67lgr + 1.84	0.53	$lg^{v(d<r)/v0}$ = 0.11lgr + 1.83	0.97
wxc2-2	$lg^{v(d<r)/v0}$ = 0.80lgr + 1.81	0.57	$lg^{v(d<r)/v0}$ = 0.11lgr + 1.81	0.94
wxc2-3	$lg^{v(d<r)/v0}$ = 0.94lgr + 1.95	0.44	$lg^{v(d<r)/v0}$ = 0.06lgr + 1.90	0.94
wxc2-4	$lg^{v(d<r)/v0}$ = 0.69lgr + 2.00	0.45	$lg^{v(d<r)/v0}$ = 0.03lgr + 1.95	0.97
wxc2-5	$lg^{v(d<r)/v0}$ = 0.70lgr + 1.85	0.54	$lg^{v(d<r)/v0}$ = 0.09lgr + 1.85	0.96

The results indicate that the overall D is primarily controlled by the dominant particle fraction. Higher clay contents corresponded to a higher D. For example, sample CS-wxc1-5 exhibited the highest D (2.81) with 93.43% clay, while NS-wxc2-4 showed a D of 2.80 with 90.04% clay. These findings are consistent with the multifractal results (Section 3.3.2), where both the information dimension (D_1) and capacity dimension (D_0) were positively correlated with the clay content and the overall fractal dimension.

3.3. Multifractal Analysis of Soil Particle Size Characteristics

3.3.1. Multifractal Behavior of Particle Size Distribution

According to multifractal theory, multifractal analysis can be conducted when the log–log plot of the partition function ($X(q, \varepsilon)$) versus the scale measure (ε) exhibits a linear relationship. Figure 7 illustrates the double-logarithmic plots of the partition function ($X(q, \varepsilon)$) and the particle size distribution measure (ε) for CS and NS in Wanxichong, with the probability density weight index (q) ranging from −10 to 10. (Due to space limitations, only the fitting results for samples wxc2-1 and wxc1-1 are presented). As shown in Figure 7, when q is negative, the slope increases with decreasing q, and the regression lines are spaced more widely. Conversely, when q is positive, the slope increases with increasing q, and the regression lines are closer together. Furthermore, the slope is negative when $q < 0$, and it is positive when $q > 0$, with q = 0 serving as the boundary. The coefficients of determination (R^2) for the linear fits range from 0.94 to 1.00, indicating that the soils in the study area exhibit clear multifractal characteristics.

3.3.2. Generalized Dimension Spectrum Characteristics

To further explore the application of fractal theory to cultivated agricultural soils and uncultivated natural soils, and to analyze differences in the multifractal characteristics of particle size distributions between cultivated and natural soil groups, the generalized dimension spectrum ($D(q)$) was calculated based on multifractal theory for $q \in [-10,10]$ with an increment of 0.5. The results are shown in Figure 8. The generalized dimension spectra of both cultivated and natural soils in the study area exhibit a monotonic decreasing trend and an inverse "S"-shaped curve. After performing multifractal transformations using 32, 16, 8, 4, and 2 partitions (boxes), notable differences in the spectrum patterns were observed between cultivated and natural soils. The spectral variation in NS is more pronounced, suggesting that NS—characterized by larger particle sizes due to natural weathering and erosion—is more sensitive to changes in q compared to cultivated soils,

which have finer particles due to anthropogenic disturbance. When $q < 0$, the variation in D(q) for NS samples is relatively small (except for sample wxc2-4), with the amplitude of change generally not exceeding 0.4. In this range, CS samples tend to have higher D(q) values than those of NS, with the difference gradually decreasing as q increases. However, when $q > 1$ and continues to increase, the gap in the D(q) values between NS and CS narrows further. This phenomenon can be attributed to two factors: first, high-density information becomes less sensitive to changes in q after multifractal partitioning, as the number of boxes is reduced in powers of two (e.g., 32 to 16 to 8, etc.), compressing the capacity dimension (D_0) accordingly and thereby limiting the variability in the D(q) values; second, the inherently small differences in high-density regions between the two soil types contribute to the convergence of D(q). Notably, samples wxc1-5 and wxc2-4 exhibit the most dramatic oscillations in their D(q) values across all samples, indicating a high sensitivity to changes in q. For wxc1-5, this is likely due to the complete absence of particles in the 0.28–0.63 μm range, which leads to zero values in the numerator during multifractal box counting for the 32-box and 16-box divisions. For wxc2-4, the extreme sensitivity of D(q) to q is associated with its highest clay content, as the abundance of clay particles strongly influences the multifractal response.

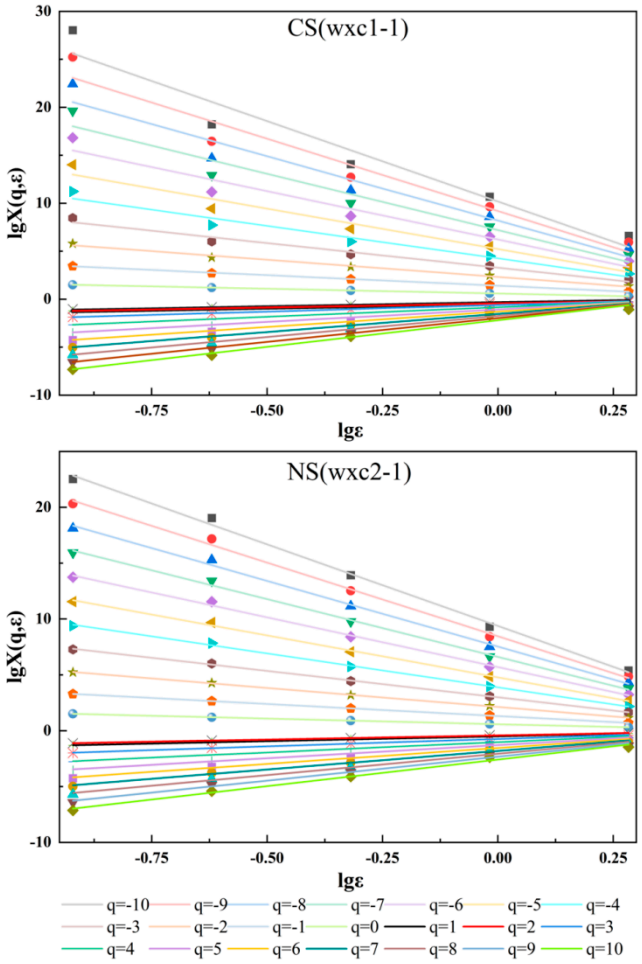

Figure 7. Log—log plots of partition functions (X(q, ε)) and measurement scales (ε) of soil particle size distribution.

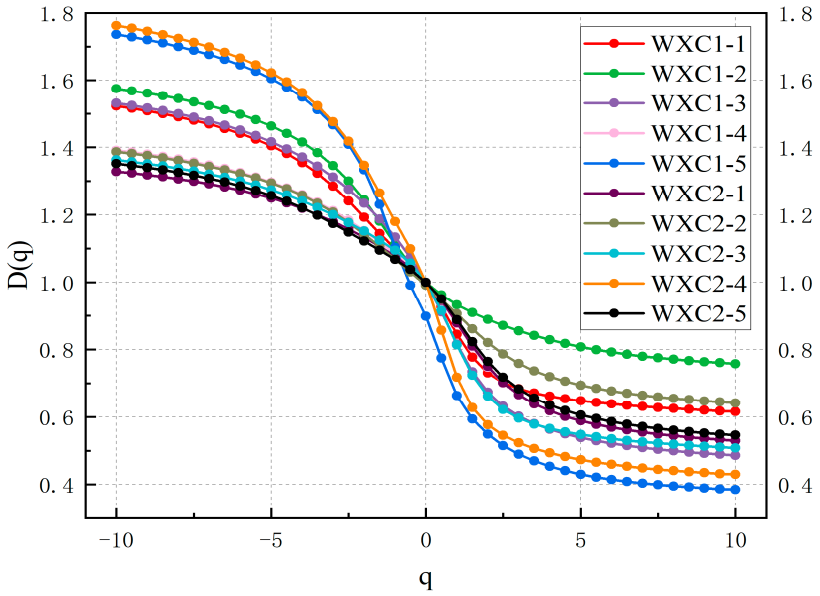

Figure 8. Generalized dimension spectrum of particle size distribution of red limestone soil samples.

The local characteristics of the soil particle size distribution in cultivated and natural soils were evaluated using the capacity dimension (D_0), information dimension (D_1), and correlation dimension (D_2). D_0 reflects the range of the particle size distribution, D_1 integrates both the distribution range and clustering, and D_2 indicates aggregation or uniformity. As shown in Table 4, the D_0 values range from 0.90 to 1.00, the D_1 values from 0.66 to 0.93, and the D_2 values from 0.57 to 0.92. The ratio D_1/D_0 lies between 0.72 and 0.93. Across all samples, the relationship $D_0 > D_1 > D_2$ holds, confirming the non-uniformity of the particle distributions and the applicability of multifractal theory. Most samples show concentrated D_0 values between 0.99 and 1.00, except for wxc1-5 ($D_0 = 0.90$), where the absence of particles in the 0.28–0.63 μm range produced zero values in the box-counting process.

Table 4. Spectral dimensions of multifractal spectral distribution of sample size distribution at sampling point.

Sample	Capacity Dimension D_0	Information Dimension D_1	Correlation Dimension D_2	D_1/D_0
wxc1-1	1.00	0.85	0.73	0.85
wxc1-2	1.00	0.93	0.90	0.93
wxc1-3	1.00	0.82	0.67	0.82
wxc1-4	1.00	0.88	0.75	0.88
wxc1-5	0.90	0.66	0.55	0.73
wxc2-1	1.00	0.88	0.75	0.88
wxc2-2	0.99	0.91	0.82	0.92
wxc2-3	1.00	0.81	0.66	0.81
wxc2-4	1.00	0.72	0.58	0.72
wxc2-5	1.00	0.89	0.76	0.89

In cultivated soils, D_1 ranges from 0.66 to 0.93 and D_2 from 0.22 to 0.90; in natural soils, D_1 ranges from 0.72 to 0.91 and D_2 from 0.58 to 0.82. The differences in D_1 and D_2 between corresponding horizons are minor, limiting their discriminative ability between land use types. To address this, the ratio D_1/D_0 has been proposed as an indicator of the particle distribution concentration [48]. Values close to 1 indicate clustering in high-density regions, while values near 0 suggest sparse distributions. The mean D_1/D_0 for

cultivated soils is 0.842, and for natural soils it is 0.844, with natural soils being slightly more concentrated. Subsurface horizons (10–20 cm), such as wxc1-2 and wxc2-2, show relatively higher D_1/D_0 values, indicating greater stability and reduced heterogeneity, consistent with their moderate clay contents (52.49%–64.79%). In contrast, deeper layers (wxc1-5 and wxc2-4) display lower D_1/D_0 values, reflecting higher heterogeneity and reduced uniformity, which correspond to their high clay contents (>90%). This suggests a negative correlation between the clay content and the D_1/D_0 ratio. The elevated clay contents in deeper layers are attributable to subtropical weathering processes. High temperatures and seasonal wet–dry cycles enhance chemical weathering, promoting carbonate leaching and the formation of secondary clays. Well-drained conditions further accelerate calcium carbonate removal and clay enrichment. These observations are consistent with the particle size characteristics and related parameter analyses.

3.3.3. Characteristics of Multifractal Spectrum Functions

The multifractal spectrum curves of the PSD in CS and NS, plotted based on α and $f(\alpha)$, are shown in Figure 9. The shape and asymmetry of the $f(\alpha)$ spectrum reflect the heterogeneity of the soil PSD. Both spectra exhibit unimodal, inverse-hook patterns with a high degree of overlap. Except for the surface CS (wxc1-1 and wxc1-2) and surface NS (wxc2-2), which had Δf values of 0.16, 0.09, and 0.23, respectively, all other layers showed $\Delta f < 0$, indicating a right-skewed spectrum. This suggests that particles with smaller volume fractions dominate in the middle and lower soil layers. In contrast, $\Delta f > 0$ in the surface layers indicates a left-skewed spectrum, where particles with larger volume fractions are also dominant but with a different distribution asymmetry. For both CS and NS, the singularity spectrum width ($\Delta\alpha$) was relatively concentrated in the range of 0.95–1.36 for surface and middle layers, while in deeper layers, it increased to 1.54–1.55. This suggests that the spectrum width ($\Delta\alpha$) may be related to the degree of soil heterogeneity. Additionally, α_0—the mean singularity strength of the multifractal structure—reflects the local density of the soil particle size distribution. Calculations show that α_0 is generally lower in NS than in CS. This finding is supported by the higher D_1/D_0 ratio observed in NS, indicating a more densely packed PSD at the local scale. This also aligns with the understanding that agricultural activities such as crop rotation, irrigation, and tillage can lead to a more uneven PSD. Furthermore, by analyzing the relationships among the information dimension (D_1), correlation dimension (D_2), and ratio D_1/D_0 (where D_0 is the capacity dimension), it was found that Δf is positively correlated with D_1, D_2, and D_1/D_0.

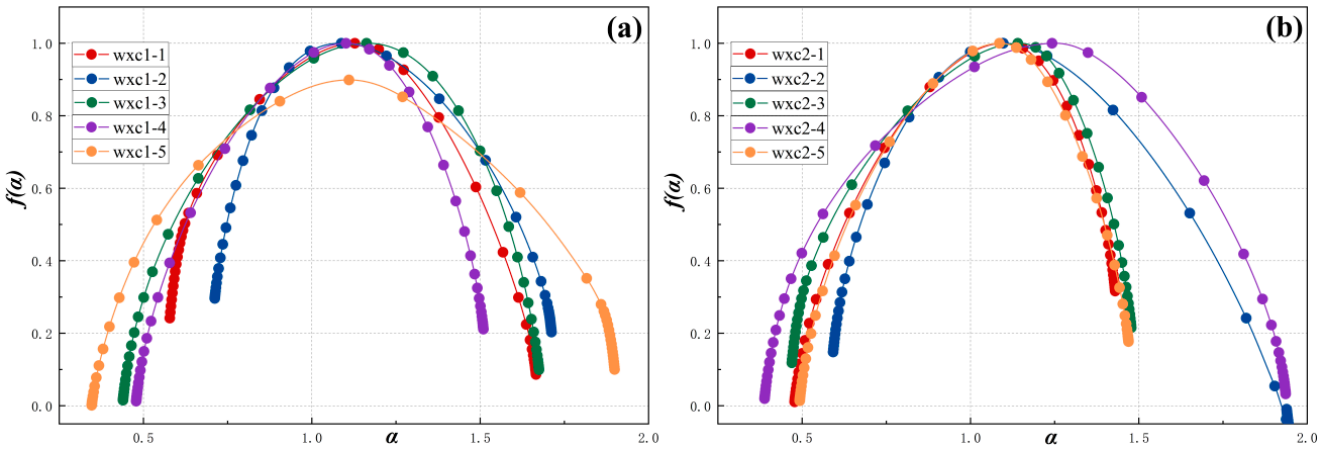

Figure 9. Multifractal spectrum function curves of particle size distribution of natural soil (**a**) and cultivated soil (**b**).

4. Discussion

4.1. Correlation Analysis and Discussion of Between Scanning Electron Microscopy (SEM) Observations and Soil Indicators

A comparative study of the particle size characteristics of lime soils from the perspective of particle size parameters and fractal theory indicates that significant differences exist in the soil particle size compositions under different land use conditions. To further reveal the intrinsic relationships among various parameters, it was necessary to conduct a correlation analysis involving the particle size composition (clay, silt, sand), particle size statistical parameters (Md, Mz, So, Sk, Ku), organic matter (OM), total nitrogen (TN), and fractal indicators (D, D_0, D_1, D_2, α_0) (results shown in Figure 10). This analysis, combined with the examination of the microstructural morphology, provides a comprehensive understanding of the role of the soil structural complexity and nutrient retention capacity, offering a theoretical basis for understanding soil quality and its evolutionary mechanisms.

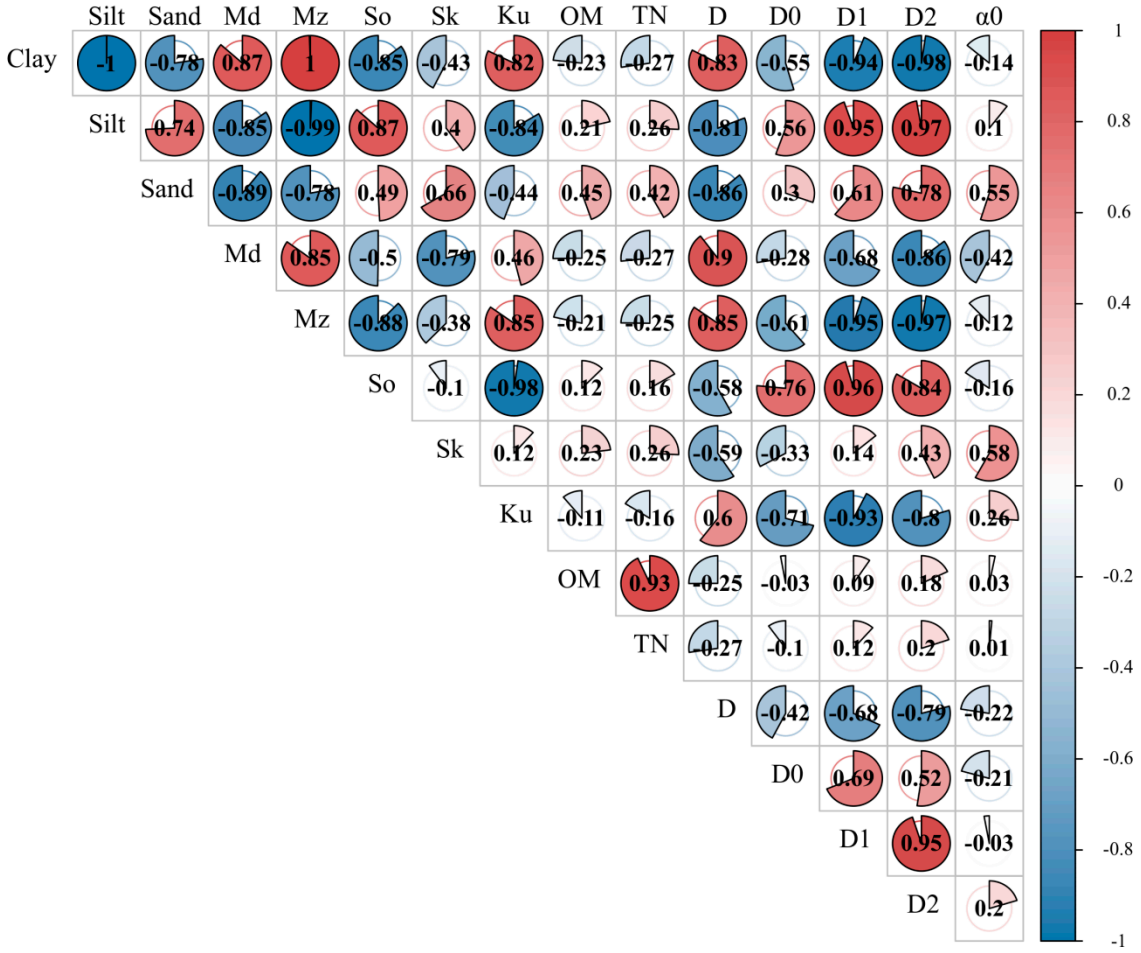

Figure 10. Pearson correlation coefficients and factor analysis between conventional soil particle size indices and multifractal parameters.

In terms of the soil texture indicators, the analysis revealed a clear complementary relationship among the contents of clay, silt, and sand in the two sample groups (CS and NS). The clay and silt contents were positively correlated, while both showed a significant negative correlation with the sand content, indicating a synergistic variation among fine particles and a substitution relationship with coarse particles. Accordingly, the median particle diameter (Md) and mean particle diameter (Mz) were negatively correlated with the sand content but positively correlated with the clay content, suggesting that soils dominated by coarser particles tend to exhibit larger-particle size characteristics. In terms of

PSD patterns, the sorting coefficient (So) is generally negatively correlated with both the mean particle size (Mz) and the median particle size (Md), indicating that poorly sorted soil samples tend to have larger average particle sizes. The skewness (Sk) and kurtosis (Ku) reflect the symmetry and peakedness of the PSD, respectively. Soils with a higher proportion of fine particles tend to exhibit fine-tail distributions, leading to significant variations in the Sk values. An increase in the Ku suggests a more sharply peaked and concentrated distribution. Overall, the relationships between the Sk, Ku, and soil fineness and sorting degree indicate intrinsic connections among particle morphology parameters. Their significant correlations reflect the coordinated variation in soil distribution characteristics. Notably, the correlation between the Sk and Ku is stronger in the NS group than that in the CS group, which may suggest that the particle distribution in NS is more stable and less structurally disturbed. In terms of the nutrient content, the organic matter (OM) and total nitrogen (TN) are generally significantly positively correlated, suggesting that these two nutrients may share a common source or transformation mechanism in the soil. Notably, the OM and TN exhibit negative correlations with the clay content but positive correlations with both the silt and sand contents. This may indicate that nutrients tend to accumulate within aggregate structures primarily composed of silt-sized particles. Agricultural practices such as tillage and irrigation may lead to the dispersion and loss of clay particles, disrupting the original aggregate structure and redistributing organic matter and nitrogen into the pore network between silt particles. Regarding the fractal indicators, strong positive correlations are observed among the various fractal parameters, reflecting their joint capacity to characterize the complexity of the soil PSD. These fractal indicators are typically negatively correlated with fine particle fractions and positively correlated with coarse fractions. In other words, samples with higher clay contents tend to exhibit higher fractal dimensions, indicating a more fragmented and complex particle structure. This suggests that the refinement of the soil PSD directly influences its fractal characteristics, revealing a close relationship between the fractal dimensions and particle size composition. This pattern is more pronounced in the CS group, implying that tillage disturbance has a significant effect on shaping the complexity of the soil particle size system.

Further combined with microstructural observations from scanning electron microscopy (SEM) images (Figure 11), it was found that in CS samples (Figure 11a,b), there was a large number of hyphal structures and distinct crop root systems, forming fine and compact aggregate structures. The hyphal networks interwoven among soil particles enhance the stability of aggregates while providing more micropores and a complex surface morphology. These features are consistent with the correlation analysis results, which showed higher fractal dimensions, higher proportions of fine particles, and elevated OM and TN contents. In contrast, NS samples (Figure 11c,d) lacked hyphae and obvious signs of biological activity. The surface aggregates appeared larger in size and more loosely structured and exhibited lower fractal dimensions and coarser-particle size characteristics. These findings are in agreement with the weaker correlations observed between the particle size statistical parameters and fractal features in the NS group. Therefore, tillage disturbance, water erosion, and plant root activity contribute to aggregate structures in CS that are more dependent on biological factors for stability. Conversely, NS, in the absence of significant disturbance and with lower biological activity, tends to form relatively stable but loosely packed coarse aggregates. These results indicate that tillage practices in agricultural systems not only determine the physical differences in the soil particle size composition but also indirectly regulate the structural complexity and fractal characteristics of the PSD by influencing the microbial activity and organic matter accumulation.

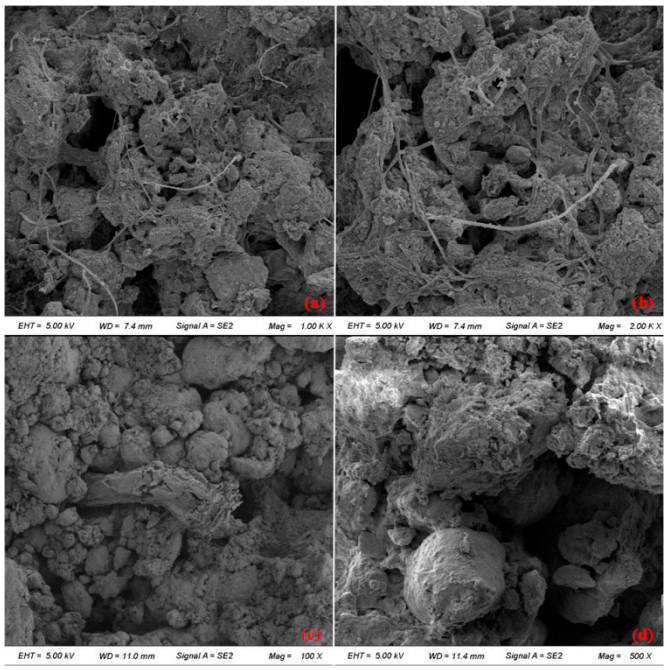

Figure 11. Microstructural features of different soil types: (**a**,**b**) CS showing extensive hyphal distribution and the formation of well-defined aggregate structures; (**c**) NS with visible plant roots and surrounding aggregate structures; (**d**) internal microstructure of NS, lacking evident biological activity and microbial presence.

Under different land use types, soils exhibit both common characteristics and distinct mechanisms in terms of their particle size compositions, nutrient contents, and fractal structures. The integration of statistical correlation analysis with microstructural observations facilitates a deeper understanding of the processes underlying the soil structural evolution and their implications for agricultural functionality. This provides a comprehensive perspective and empirical support for soil quality assessment and management.

4.2. Future Perspectives

In future research, our focus will be broadened to include calcareous soils across the wider Yunnan Province. Building upon the multifractal theoretical framework established in this study, we aim to further examine the effects of cultivation practices on the particle size distribution (PSD) of calcareous soils, with particular attention to quantifying and comparing the multifractal spectra and related parameters between natural and cultivated soils. This expanded scope will not only facilitate a more comprehensive understanding of the spatial variability in and land use-driven transformations of calcareous soils under diverse natural geographic conditions, but it will also provide a solid empirical foundation for the formulation of sustainable agricultural management strategies. Ultimately, our objective is to extend the applicability of the present findings to agricultural systems throughout calcareous soil distribution areas, thereby enhancing the universality and practical relevance of our conclusions for both scientific research and land use policy development.

5. Conclusions

(1) The multifractal analysis of the PSD confirms that both cultivated and natural calcareous soils exhibit heterogeneous and non-uniform structures. Cultivation alters soil particle size characteristics, thereby broadening the distribution range and modifying multifractal behaviors, whereas natural soils maintain relatively stable and concentrated particle distributions.

(2) The clay content is the dominant factor influencing the fractal dimensions (D, D_0, D_1, D_2) across both land uses. Yet, the degree of correlation differs; in cultivated soils, frequent tillage and fertilization amplify the variability associated with clay, while in natural soils, clay enrichment is more closely linked to long-term pedogenic processes and stable aggregation.

(3) The comparison between cultivated and natural soils highlights the contrasting influences of human activity and natural processes. Cultivated soils generally contain higher organic matter and total nitrogen due to fertilization and crop residue return, which not only enhance aggregation but also intensify heterogeneity in the PSD. In contrast, natural soils, despite their lower nutrient contents, maintain more uniform structural characteristics shaped by vegetation cover and reduced disturbance.

(4) The integration of the fractal and multifractal approaches enables the identification of subtle differences between cultivated and natural soils that are not fully captured by traditional PSD indices. This suggests that fractal metrics can serve as sensitive indicators for monitoring land use-driven changes in soil quality.

(5) From an applied perspective, the findings provide empirical evidence to support sustainable land management in calcareous soil regions. By linking soil PSD characteristics and fractal theory features with nutrient status, this study offers insights for optimizing cultivation practices aimed at maintaining soil fertility and mitigating degradation risks. Future research should extend this framework across broader spatial scales and diverse land use systems to enhance its applicability in guiding soil conservation and agricultural policy.

Author Contributions: Z.X. was responsible for the review and editing of the manuscript, as well as for providing software guidance. Y.L. contributed to the writing of the original draft. Y.L., H.Y., J.B., X.D., and Y.Z. were responsible for conducting the experimental operations. All authors have read and agreed to the published version of the manuscript.

Funding: This research was financially supported by the Yunnan Natural Science Foundation Project (202401AT070119).

Data Availability Statement: Data is contained within the article. The original contributions presented in this study are included in the article; further inquiries can be directed to the corresponding author.

Conflicts of Interest: The authors declare no conflicts of interest.

References

1. Wang, P.; Su, X.; Zhou, Z.; Wang, N.; Liu, J.; Zhu, B. Differential Effects of Soil Texture and Root Traits on the Spatial Variability of Soil Infiltrability under Natural Revegetation in the Loess Plateau of China. *CATENA* **2023**, *220*, 106693. [CrossRef]
2. Huang, B.; Sun, W.; Zhao, Y.; Zhu, J.; Yang, R.; Zou, Z.; Ding, F.; Su, J. Temporal and Spatial Variability of Soil Organic Matter and Total Nitrogen in an Agricultural Ecosystem as Affected by Farming Practices. *Geoderma* **2007**, *139*, 336–345. [CrossRef]
3. Hu, X.; Dong, C.; Zhang, Y. Impacts of Cropland Utilization Patterns on the Sustainable Use Efficiency of Cropland Based on the Human–Land Perspective. *Land* **2024**, *13*, 863. [CrossRef]
4. Institute of Soil Science, Chinese Academy of Sciences. *Soil Physical and Chemical Analysis*; Shanghai Science and Technology Press: Shanghai, China, 1978; pp. 469–510. (In Chinese)
5. Wei, Y.; Wu, X.; Xia, J.; Shen, X.; Cai, C. Variation of Soil Aggregation along the Weathering Gradient: Comparison of Grain Size Distribution under Different Disruptive Forces. *PLoS ONE* **2016**, *11*, e0160960. [CrossRef]
6. Wei, Y.; Wu, X.; Cai, C. Splash Erosion of Clay–Sand Mixtures and Its Relationship with Soil Physical Properties: The Effects of Particle Size Distribution on Soil Structure. *CATENA* **2015**, *135*, 254–262. [CrossRef]
7. Liu, Z.; Dugan, B.; Masiello, C.A.; Gonnermann, H.M. Biochar Particle Size, Shape, and Porosity Act Together to Influence Soil Water Properties. *PLoS ONE* **2017**, *12*, e0179079. [CrossRef] [PubMed]
8. Huang, B.; Yuan, Z.; Li, D.; Zheng, M.; Nie, X.; Liao, Y. Effects of Soil Particle Size on the Adsorption, Distribution, and Migration Behaviors of Heavy Metal(Loid)s in Soil: A Review. *Environ. Sci. Process. Impacts* **2020**, *22*, 1596–1615. [CrossRef]

9. Zhou, G.; Fan, K.; Gao, S.; Chang, D.; Li, G.; Liang, T.; Liang, H.; Li, S.; Zhang, J.; Che, Z.; et al. Green Manuring Relocates Microbiomes in Driving the Soil Functionality of Nitrogen Cycling to Obtain Preferable Grain Yields in Thirty Years. *Sci. China Life Sci.* **2023**, *67*, 596–610. [CrossRef]
10. Wu, X.; Wei, Y.; Cai, C.; Yuan, Z.; Liao, Y.; Li, D. Effects of Erosion-Induced Land Degradation on Effective Sediment Size Characteristics in Sheet Erosion. *CATENA* **2020**, *195*, 104843. [CrossRef]
11. Koiter, A.J.; Owens, P.N.; Petticrew, E.L.; Lobb, D.A. The Role of Soil Surface Properties on the Particle Size and Carbon Selectivity of Interrill Erosion in Agricultural Landscapes. *CATENA* **2017**, *153*, 194–206. [CrossRef]
12. Guglielmo, M.; Tang, F.H.M.; Pasut, C.; Maggi, F. SOIL-WATERGRIDS, Mapping Dynamic Changes in Soil Moisture and Depth of Water Table from 1970 to 2014. *Sci. Data* **2021**, *8*, 263. [CrossRef] [PubMed]
13. Furtak, K.; Wolińska, A. The Impact of Extreme Weather Events as a Consequence of Climate Change on the Soil Moisture and on the Quality of the Soil Environment and Agriculture—A Review. *CATENA* **2023**, *231*, 107378. [CrossRef]
14. Ghanbarian-Alavijeh, B.; Millán, H. The Relationship between Surface Fractal Dimension and Soil Water Content at Permanent Wilting Point. *Geoderma* **2009**, *151*, 224–232. [CrossRef]
15. Bruun, E.W.; Petersen, C.T.; Hansen, E.; Holm, J.K.; Hauggaard-Nielsen, H. Biochar Amendment to Coarse Sandy Subsoil Improves Root Growth and Increases Water Retention. *Soil. Use Manag.* **2014**, *30*, 109–118. [CrossRef]
16. Shen, P.; Zhang, L.M.; Zhu, H. Rainfall Infiltration in a Landslide Soil Deposit: Importance of Inverse Particle Segregation. *Eng. Geol.* **2016**, *205*, 116–132. [CrossRef]
17. Lu, C.; Li, L.; Xu, J.; Zhao, H.; Chen, M. Research on the Critical Value of Sand Permeability Particle Size and Its Permeability Law after Mixing. *Water* **2024**, *16*, 393. [CrossRef]
18. Luo, G.; Friman, V.-P.; Chen, H.; Liu, M.; Wang, M.; Guo, S.; Ling, N.; Shen, Q. Long-Term Fertilization Regimes Drive the Abundance and Composition of N-Cycling-Related Prokaryotic Groups via Soil Particle-Size Differentiation. *Soil. Biol. Biochem.* **2018**, *116*, 213–223. [CrossRef]
19. Jozedaemi, E.; Golchin, A. Changes in Aggregate-Associated Carbon and Microbial Respiration Affected by Aggregate Size, Soil Depth, and Altitude in a Forest Soil. *CATENA* **2024**, *234*, 107567. [CrossRef]
20. Chen, T.; Shi, Z.; Wen, A. Concentrations and Stoichiometric Characteristics of C, N, and P in Purple Soil of Agricultural Land in the Three Gorges Reservoir Region, China. *Sustainability* **2023**, *15*, 2434. [CrossRef]
21. Mandelbrot, B.B. Multifractal measures, especially for the geophysicist. *Pure Appl. Geophys.* **1989**, *131*, 5–42. [CrossRef]
22. Jia, Y.; Feng, Y.; Zhang, X.; Sun, X. Multifractal Analysis of Temporal Variation in Soil Pore Distribution. *Agronomy* **2024**, *15*, 37. [CrossRef]
23. Cohen, S.; Willgoose, G.; Svoray, T.; Hancock, G.; Sela, S. The Effects of Sediment Transport, Weathering, and Aeolian Mechanisms on Soil Evolution. *JGR Earth Surf.* **2015**, *120*, 260–274. [CrossRef]
24. Mohammadi, M.; Shabanpour, M.; Mohammadi, M.H.; Davatgar, N. Characterizing Spatial Variability of Soil Textural Fractions and Fractal Parameters Derived from Particle Size Distributions. *Pedosphere* **2019**, *29*, 224–234. [CrossRef]
25. Stanchi, S.; Bonifacio, E.; Zanini, E. Mass-size fractal dimension of primary and aggregated particles and soil profile development. *Soil. Sci.* **2008**, *173*, 87–95. [CrossRef]
26. Tian, Z.; Pan, Y.; Chen, M.; Zhang, S.; Chen, Y. The Relationships between Fractal Parameters of Soil Particle Size and Heavy-Metal Content on Alluvial-Proluvial Fan. *J. Contam. Hydrol.* **2023**, *254*, 104140. [CrossRef]
27. Wang, J.; Li, W.; Mu, M.; Chen, J.; Li, Y.; Liu, H.; Su, Q. Particle Size Composition Characteristics of Weathered Debris from Grey–Green Slate under the Action of Freeze–Thaw and Dry–Wet Cycles. *Sci. Rep.* **2023**, *13*, 1421. [CrossRef]
28. Rodríguez-Lado, L.; Lado, M. Relation between Soil Forming Factors and Scaling Properties of Particle Size Distributions Derived from Multifractal Analysis in Topsoils from Galicia (NW Spain). *Geoderma* **2017**, *287*, 147–156. [CrossRef]
29. Guan, X.; Yang, P.; Ren, S.; Li, X.; Lü, Y. Analysis of heterogeneity in loam particle-size distribution based on multifractal theory. *J. Basic. Sci. Eng.* **2009**, *17*, 196–205. (In Chinese)
30. Gao, Y.; Liao, L.; Wang, J.; Wan, Q.; Liu, G.; Zhang, C. Effects of grazing exclusion on multifractal characteristics of soil particle-size distribution in semi-arid grasslands of the Loess Plateau. *J. Soil. Water Conserv.* **2021**, *35*, 310–318, 326. (In Chinese) [CrossRef]
31. Su, W.; Gao, Y.; Gao, P.; Dong, X.; Wang, G.; Dun, X.; Xu, J. Effects of different vegetation restoration types on the fractal characteristics of soil particles in earthy-rocky mountain area of northern China. *Forests* **2022**, *13*, 1246. [CrossRef]
32. Li, J.; Bao, Y.; Wei, J.; He, X.; Tang, Q.; Wu, S.; Huang, P.; Ma, M.; Zhou, P.; Wang, M. Scaling properties of particle-size distributions of purple soils in a small agricultural watershed: A multifractal analysis. *CATENA* **2022**, *215*, 106326. [CrossRef]
33. Sun, Z.; Ma, X.; Chen, Y. Single and multifractal characteristics of soil particle size distribution in different forestlands in a typical karst area of Guangxi. *Bull. Soil. Water Conserv.* **2025**, *45*, 10–19. [CrossRef]
34. Zhu, R.; Xiao, S.; Zhang, G. Fractal characteristics of soil particles under different vegetation restoration in karst rocky desertification areas. *J. Jiangxi Agric. Univ.* **2024**, *46*, 516–529. [CrossRef]
35. Gao, H.; Zhang, J. Statistical analysis of physical and mechanical properties of secondary red clay in Chenggong, Kunming. *Coal Geol. Explor.* **2021**, *49*, 174–181. (In Chinese)

36. Yu, M.; Jin, H.; Li, Q.; Yao, Y.; Zhang, Z. Accounting study of Gross Ecosystem Product (GEP) in Chenggong District. *West. For. Sci.* **2020**, *49*, 41–48+55. (In Chinese) [CrossRef]
37. Hong, Q.; Li, Q.; Feng, X.; Dai, Y.; Hao, J.; Ai, D. Multifunctional evolution and optimized zoning of characteristic agriculture in plateau mountainous areas under the context of high-quality development: A case study of Yunnan Province. *J. China Agric. Univ.* **2024**, *29*, 193–208. (In Chinese)
38. *GB/T 42363-2023*; Soil Quality—Pretreatment of Samples for Physico-Chemical Analysis. Standards Press of China: Beijing, China, 2023. (In Chinese)
39. Bittelli, M.; Pellegrini, S.; Olmi, R.; Andrenelli, M.C.; Simonetti, G.; Borrelli, E.; Morari, F. Experimental evidence of laser diffraction accuracy for particle size analysis. *Geoderma* **2022**, *409*, 115627. [CrossRef]
40. Wei, W.; Liu, T.; Zhang, S.; Shen, L.; Wang, X.; Li, L.; Zhu, Y.; Zhang, W. Root spatial distribution and belowground competition in an apple/ryegrass agroforestry system. *Agric. Syst.* **2024**, *215*, 103869. [CrossRef]
41. Bremner, J.M. Determination of nitrogen in soil by the Kjeldahl method. *J. Agric. Sci.* **1960**, *55*, 11–33. [CrossRef]
42. Ding, Y.; Gao, Y.; Meng, Z.; Narengeerile Huang, X.; Sun, X.; Wu, H.; Dang, X.; Wang, M. Grain-size characteristics of wind-eroded surface particles in the Xilamuren desert steppe. *Soils* **2016**, *48*, 803–812. (In Chinese) [CrossRef]
43. Gao, G.; Ding, G.; Zhao, Y.; Feng, W.; Bao, Y.; Liu, Z. Effects of biological soil crust development on soil particle-size characteristics in the Mu Us Sandy Land. *Trans. Chin. Soc. Agric. Mach.* **2014**, *45*, 115–120. (In Chinese)
44. Qi, F.; Zhang, R.; Liu, X.; Niu, Y.; Zhang, H.; Li, H.; Li, J.; Wang, B.; Zhang, G. Soil particle size distribution characteristics of different land-use types in the Funiu mountainous region. *Soil. Tillage Res.* **2018**, *184*, 45–51. [CrossRef]
45. Wang, Z.; Hasi, E.; Han, X.; Qingda, M. Fractal characterization of soil particle size distribution under different land use patterns on the north slope of Wula Mountain in China. *J. Soils Sediments* **2024**, *24*, 1148–1164. [CrossRef]
46. Dai, L.; Wang, G.; He, Y. The Relationship between Soil Structure and Water Characteristics Based on Fractal Theory. *Earth Sci.* **2021**, *46*, 3410–3420. [CrossRef]
47. Tian, Z.; Zhang, S.P.; Wang, X.; Fang, R.D.; Zheng, J.D. Fractal characteristics of soil particle size distribution under different land use patterns in Longji Terraced Fields. *Res. Agric. Mod.* **2023**, *44*, 724–735. [CrossRef]
48. Wang, D.; Fu, B.J.; Chen, L.D.; Zhao, W.W.; Wang, Y.F. Fractal analysis of soil particle size under different land use types: A case study of the loess hilly-gully region. *Acta Ecol. Sin.* **2007**, *27*, 3081–3089.
49. Wan, Q.; Wang, J.; Wang, X.T.; Liu, G.; Zhang, C. Effects of different grassland utilization patterns on soil particle size fractal characteristics in the Qinghai-Tibet Plateau. *Acta Ecol. Sin.* **2022**, *42*, 1716–1726.
50. Montero, E.S. Rényi dimensions analysis of soil particle-size distributions. *Ecol. Model.* **2005**, *182*, 305–315. [CrossRef]
51. Xia, S.; Song, Z.; Jeyakumar, P.; Bolan, N.; Wang, H. Characteristics and applications of biochar for remediating Cr(VI)-contaminated soils and wastewater. *Environ. Geochem. Health* **2019**, *42*, 1543–1567. [CrossRef]
52. Sun, C.; Liu, G.; Xue, S. Response of soil multifractal characteristics and erodibility to 15-year fertilization on cropland in the Loess Plateau, China. *Arch. Agron. Soil. Sci.* **2016**, *63*, 956–968. [CrossRef]
53. Wang, Y.; Meng, Z.J.; Seriengbilige Ding, Y.L.; Wang, Z.Y.; Wan, F.; Wu, X.L. Study on surface soil particle size distribution characteristics in semi-arid farmland based on multifractal theory. *Soils* **2018**, *50*, 826–831. [CrossRef]
54. Sun, M.; Sun, N.; Huang, Y.X.; Xu, M.G.; Wang, B.R.; Zhang, X.B. Multifractal characteristics of particle size distribution in red soil under long-term different fertilization. *Sci. Agric. Sin.* **2014**, *47*, 2173–2181.
55. Chang, H.T.; Zhao, J.; Liu, J.N.; Liu, R.T.; Luo, Y.X.; Zhang, J. Effects of conversion of cropland to forest and grassland on soil physicochemical properties and fractal characteristics: A case study of the Ningxia desert steppe. *Acta Prataculturae Sin.* **2019**, *28*, 14–25.
56. Wu, X.; Wang, S.; Cheng, H.; Yang, Y. Variation of soil organic matter with particle size in the wind erosion region of northern China. *CATENA* **2024**, *241*, 108025. [CrossRef]
57. Cheng, L.; Song, Y.; Yang, L.; Chang, H.; Wu, Y.; Long, H.; Miao, X.; Dong, Z. Variations of the Intensity of the Siberian High During the Last Glacial Revealed by the Sorting Coefficient of Loess-Paleosol Deposits in Eastern Central Asia. *Paleoceanogr. Paleoclimatology* **2022**, *37*, e2022PA004468. [CrossRef]
58. Wang, Z.D.; Yu, D.S.; Wang, W.G.; Luo, F.S.; Yang, J.Y. Relationship between fractal characteristics of particle size and sedimentology of surface sediments in Quanzhou Bay. *Trans. Oceanol. Limnol.* **2021**, *43*, 82–88. [CrossRef]

Disclaimer/Publisher's Note: The statements, opinions and data contained in all publications are solely those of the individual author(s) and contributor(s) and not of MDPI and/or the editor(s). MDPI and/or the editor(s) disclaim responsibility for any injury to people or property resulting from any ideas, methods, instructions or products referred to in the content.